Bull. Mater. Sci., Vol. 30, No. 3, June 2007, pp. 247–254. © Indian Academy of Sciences.

Structural and optical properties of ZnO films grown on silicon and their applications in MOS devices in conjunction with ZrO_2 as a gate dielectric

S K NANDI[†], S CHAKRABORTY, M K BERA and C K MAITI*

Department of Electronics and ECE, Indian Institute of Technology, Kharagpur 721 302, India
[†]Department of Electronics Engineering and Institute of Electronics, National Chiao Tung University, Hsinchu 300, Taiwan, R.O.C.

MS received 3 July 2006; revised 20 April 2007

Abstract. Photoluminescence (PL) properties of undoped ZnO thin films grown by rf magnetron sputtering on silicon substrates have been investigated. ZnO/Si substrates are characterized by Rutherford backscattering (RBS), X-ray diffraction (XRD), Fourier transform infrared (FTIR), and X-ray photoelectron spectroscopy (XPS). ZrO_2 thin films have been deposited on ZnO using microwave plasma enhanced chemical vapour deposition at a low temperature (150°C). Using metal insulator semiconductor (MIS) capacitor structures, the reliability and the leakage current characteristics of ZrO_2 films have been studied both at room and high temperatures. Schottky conduction mechanism is found to dominate the current conduction at a high temperature. Good electrical and reliability properties suggest the suitability of deposited ZrO_2 thin films as an alternative as gate dielectric on ZnO/*n*-Si heterostructure for future device applications.

Keywords. ZnO; ZrO_2; PECVD; high-*k* gate dielectric; conduction mechanism.

1. Introduction

Now a days, ZnO film is receiving increased attention for various microelectronic applications. It has potential uses in photo detectors (Liu *et al* 2000), solar cells, and light emitting diodes (LEDs) (Jeong *et al* 2006). ZnO is a II–VI compound *n*-type semiconductor with a wide direct band of 3·3 eV (at room temperature) (Tang *et al* 2006) and has a hexagonal quartzite structure with space group $P6_3mc$, and cell parameters of $a = 0{\cdot}3250$ nm, $c = 0{\cdot}5206$ nm (Kubo *et al* 2000). It has a large exciton binding energy of 60 meV (Marotti *et al* 2004) which indicates that ZnO is the material with most potential to realize the next generation UV semiconductor laser. Silicon is not only of interest for the integration of optoelectronic devices but is also cheaper and easier to cleave in comparison with sapphire, which is widely used as substrate in the deposition of ZnO film (Xu *et al* 2005).

The current trends in silicon metal–oxide–semiconductor field effect transistors (MOSFETs) scaling have indicated that new generation of devices are necessary beyond 2010 or so. As the device dimensions are scaled down, the gate dielectric thickness needs to be scaled and a 15 Å thick SiO_2 will be necessary soon. However, due to high direct tunneling current and reliability concerns, conventional thermally grown silicon dioxide (SiO_2) cannot be used as the gate dielectric and an alternative is being researched into. High dielectric constant (high-*k*) gate dielectrics are needed to replace SiO_2 by providing a physically thicker layer and still maintain the same gate capacitance, while reducing the tunneling current.

Alternative high-*k* materials such as HfO_2, Ta_2O_5, ZrO_2, TiO_2 etc are currently under intense investigation. Among them ZrO_2 is a promising candidate for replacement of SiO_2 because it is a very promising material for optical (for its high reflective index, low absorption coefficient, etc) and mechanical (for its hardness, durability, and low chemical reactivity) applications (Balog *et al* 1977; Russak *et al* 1989; Khawaja *et al* 1993; Kralik *et al* 1998; Cameron and George 1999). In fact, ZrO_2 has some very attractive properties for microelectronics applications. It has a wide band gap of 5·16–7·1 eV (Balog *et al* 1977; French *et al* 1994); this wide band gap could result in high barrier height for tunneling and hence reduces the leakage current. It has a dielectric constant in the range 15–22, which is high enough to achieve lower equivalent oxide thickness (EOT).

To produce the electronic devices using ZnO films, it is essential to study the electrical and other properties such as structural reactions with high-*k* gate dielectrics deposited on it. Usually, the metal insulator semiconductor (MIS) structures are used for this purpose. For the realization of electronic devices, it is also important to understand the

*Author for correspondence (ckm@ece.iitkgp.ernet.in)

stability, formation kinetics of the dielectric films and also their reliability on thin ZnO films. However, very little is known about the interfacial properties of gate dielectrics deposited on thin ZnO films. Chemical vapour deposition (CVD) techniques are commonly used to deposit dielectric films due to their superior step coverage over physical vapour deposition processes. The plasma enhanced CVD (PECVD) process has a distinct advantage over other thermal CVD methods in which a high deposition rate can be achieved at a low substrate temperature (Ray *et al* 1996; Raoux *et al* 1997).

In the present study, ZnO films were deposited by the conventional rf magnetron sputtering on silicon substrates, and the ZnO/Si structures are characterized by RBS, XRD, PL and FTIR. To the best of our knowledge, there has been no report on the electrical and interfacial properties of ZrO_2/ZnO/*n*-Si structures. In this paper, we report on the deposition of thin high-*k* ZrO_2 films at a low temperature on ZnO/*n*-Si substrates and the electrical properties of thin ZrO_2 films as a gate dielectric both at room and high temperatures.

2. Experimental

In this study, undoped ZnO (100 nm thick) thin films were grown on *n*-Si (100) at 450°C by rf magnetron sputtering of sintered commercial 2-inch ZnO targets (purity, ~99·99%). Ar was introduced as a plasma gas and working pressure was 10 mTorr. After standard cleaning (RCA) of the ZnO/*n*-type Si substrates followed by a dip in 1% HF, ZrO_2 films were deposited by microwave (700 watt, 2·45 GHz) plasma cavity discharge system at a pressure of 500 mTorr and temperature of 150°C. For ZrO_2 films deposition, metalorganic zirconium tetratert butoxide [$Zr(OC(CH_3)_3)_4$] compound and O_2 were used as the source materials. The thickness of ZrO_2 films (15 nm) was determined using a single wavelength (632·8 nm) ellipsometer (Model: Gaertner L-117). The electrical properties of the deposited films were studied using Al/ZrO_2/ZnO/*n*-Si MIS capacitors with an Al gate (area: $1{\cdot}96 \times 10^{-3}$ cm^2). The capacitance–voltage (*C*–*V*), conductance–voltage (*G*–*V*), and current–voltage (*I*–*V*) were measured using HP-4061A semiconductor test system and HP-4145B DC parameter analyser, respectively.

3. Results and discussion

Rutherford backscattering (RBS) analysis was carried out to estimate the composition and thickness of the films. 2 MeV He^{+2} beams, attained through a charge exchange process with a stripper nitrogen gas, is normally used for the RBS and channeling measurements. The energy momentum of the beam is gained from a 90° analysing magnet and the beam is directed to the scattering chamber through a switching magnet. The beam is collimated by a pair of collimators of diameter, 1 mm, separated by a distance of about half a meter. This is done to reduce the divergence of the beam, which is important for channeling measurements. The surface barrier detector (SBD) (resolution, 25 keV) can detect scattered particles over a scattering range of 0–170°. The solid angle subtended by SBD is maintained around 2×10^{-3} steradian with the target. The beam current is in the range 5–20 nA. The sample position with respect to the beam can be varied vertically without breaking the vacuum. The data are collected by a MCDWIN (Version-1.0) multichannel analyser attached to a data acquisition computer. Figure 1 shows a typical RBS spectrum of ZnO/Si sample as described above. The scattered He^{+2} from the ZnO layer appears at higher energies (channel nos. 715–750) while those from the bulk Si substrate appear at lower energies (channel nos. 500–525). The experimental spectra were simulated using GISA 3.99. The thickness of ZnO layer was estimated to be 100·5 nm.

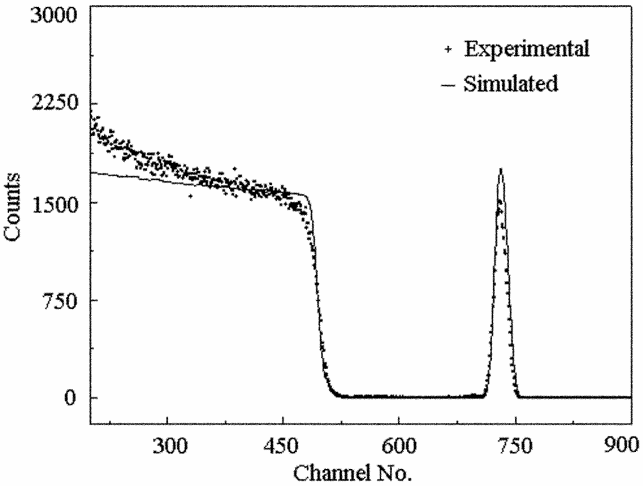

Figure 1. 2 MeV $^4He^{2+}$ Rutherford backscattering spectra of ZnO/Si sample: (+++) experimental and (---) simulation.

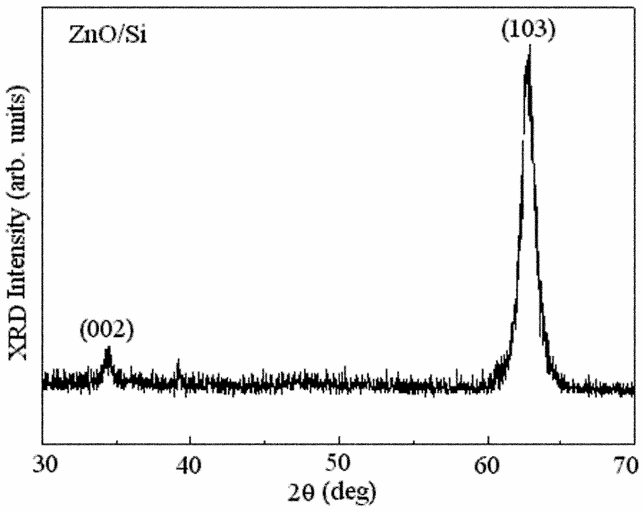

Figure 2. X-ray diffraction pattern of the as-grown ZnO thin film at 450°C and rf power, 100 W.

ZnO films usually exhibit (002) orientation with *c*-axis perpendicular to the substrate due to the lowest surface free energy for (002) plane. Another preferred orientation, however, is difficult to form, but is of interest. It is seen that ZnO films with (103) orientations are deposited by rf magnetron sputtering as shown in figure 2. The angular peak position of deposited films with (002) orientation is located at $2\theta = 34{\cdot}1°$ (Nandi *et al* 2002). From XRD study it is clear that the deposited ZnO film is polycrystalline in nature. Now one can easily estimate the average crystallite size using the Scherrer's equation:

$$D = \frac{0{\cdot}9\lambda}{\beta \cos\theta},$$

where λ is the wavelength of radiation used in XRD study, β the FWHM of the peak corresponding to (*hkl*) plane and θ the Bragg angle at peak position. Using the above relation the average crystallite size for (103) plane was estimated to be ~19·2 Å.

To investigate the optical properties of films, photoluminescence (PL) measurements were performed. Although there are many reports concerning the luminescence properties of ZnO, for bulk samples and powder phosphors, usually pressed in pellets and sintered at high temperature (Vanheusden *et al* 1996), there are only a few reports concerning PL of ZnO films. Recently, ZnO films have attracted much interest because of its potential commercial application in ultraviolet (UV) laser since its optically pumped UV lasing was found at room temperature (Bagnall *et al* 1997) and the PL properties of ZnO films have been studied widely. However, the excitation mechanism is not yet clear because a laser is usually used as the exciting source in most PL studies. Here, we observed the emission and excitation spectra of ZnO film using 325 nm HeCd laser as the exciting source with energy, 20 mW.

Under the 325 nm excitation, the PL emission spectra of a ZnO film at different temperatures are shown in figure 3. From the emission spectra, it is clearly found that there are two emission bands which peaked at 380 nm (UV band) and 502 nm (green band) for all. The origins of the 380 nm and 502 nm bands have been ascribed to the band edge radiative recombination and intrinsic defects (mostly O vacancy) of ZnO, respectively and many workers have reported similar results (Tanaka *et al* 1995; Gorla *et al* 1999; Shi *et al* 1999). From figure 3, it can be seen that the intensity of 380 nm and 502 nm emission decreases when the sample temperature is increased. When the temperature is above 100 K, the 502 nm emission disappears. Also, the intensity of 380 nm increases as the sample temperature increases until it reaches 200 K and then decreases. The

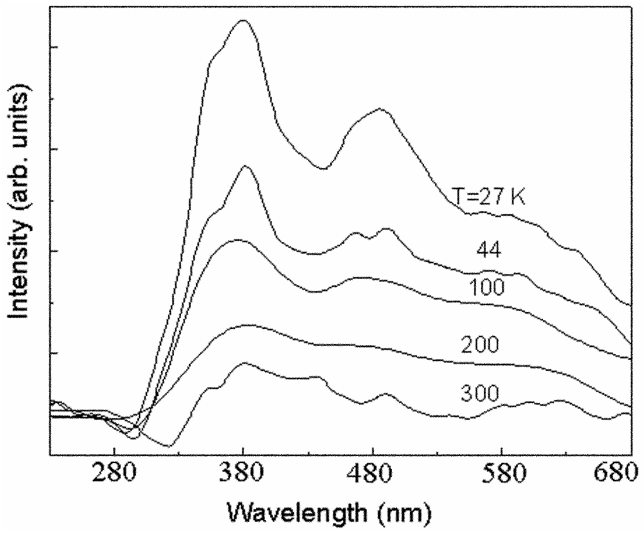

Figure 3. Emission PL spectra of ZnO films at different temperatures.

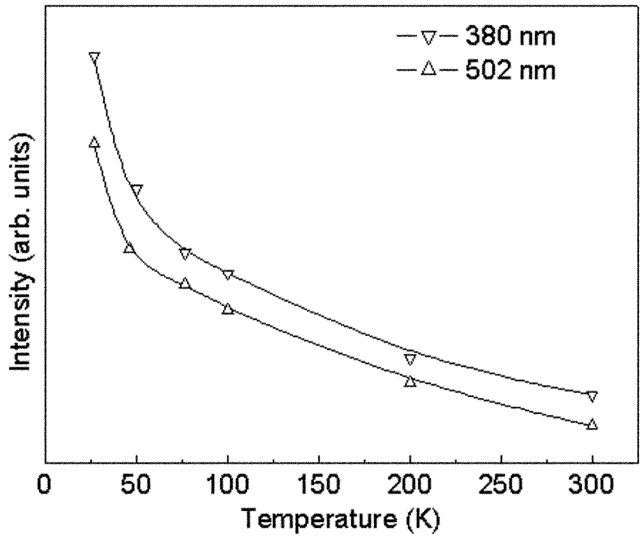

Figure 4. Integrated intensities of 380 nm and 502 nm emission peaks at different temperatures.

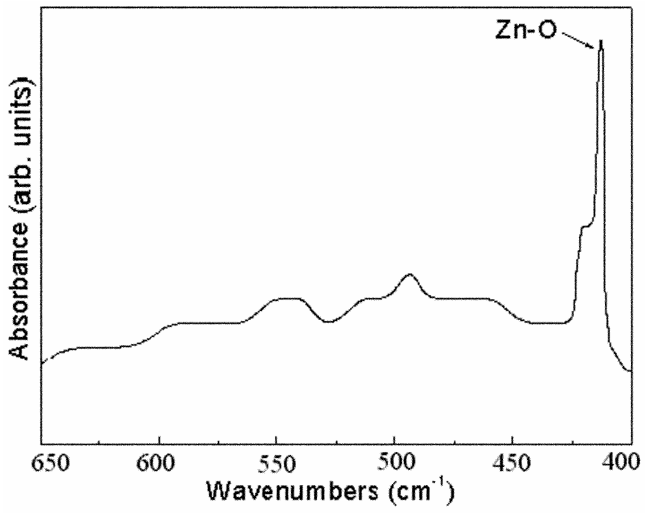

Figure 5. FTIR spectrum of ZnO film deposited on silicon substrate at 450°C.

integrated intensities of 380 and 502 nm emission peaks at different temperatures are shown in figure 4, which were calculated from the area under the curves of related emission peaks in figure 3.

Fourier transform infrared spectrum is the characteristic of a particular compound providing information about its functional groups, molecular geometry and inter/intra-molecular interactions. The infrared spectrophotometer provides a record of the infrared absorbency or transmittance of a sample as a function of wave number. The frequencies at which absorption occurs may indicate the type of functional groups present in the substance. Fourier transform infrared spectroscopic (FTIR) measurements in the wave number range between 400 and 1000 cm^{-1} were carried out using Nicolet Magana IR750, FTIR spectrometer. In this spectrum (shown in figure 5), the absorbance band is situated at 411·5 cm^{-1}. This band corresponded to the Zn–O stretching vibration for a tetrahedral surrounding of the zinc atoms (Bachari *et al* 2001).

XPS study was carried out using a model ESCALAB MKII high vacuum system equipped with a concentric hemispherical analyser (VG Microtech) with a residual gas pressure of ~1×10^{-8} Pa. MgK_α X-ray ($h\nu$ = 1253·6 eV) radiation was used to excite the photoelectrons at an angle of 30° between the analyser axis and the sample normal. All spectra were taken at 300 K (room temperature). The broad energy XPS spectra of the films are shown in figure 6(a). It is observed that peaks are found to be at 100 eV for Si 2*p*, 149 eV for Si 2*s*, 182 eV for Zr 3*d*, 284 eV for C 1*s*, 532 eV for O 1*s*, 1022 eV for Zn $2p_{3/2}$ and 1045 eV for Zn $2p_{1/2}$. Figures 6(b) and (c) show the high-resolution XPS spectra of O 1*s* and Zr 3*d*, respectively. Figure 6(b) shows the measured O 1*s* peak, which can be deconvoluted into two sub peaks at 531·8 eV and 529·7 eV, assigned to –OH and Zn–O bonding, respectively (Ayouchi *et al* 2003). Figure 6(c) shows the core-level spectrum of Zr 3*d* at binding energies, 182·3 eV for Zr $3d_{5/2}$ and 184·6 eV for Zr $3d_{3/2}$. The peak of Zr $3d_{5/2}$ at

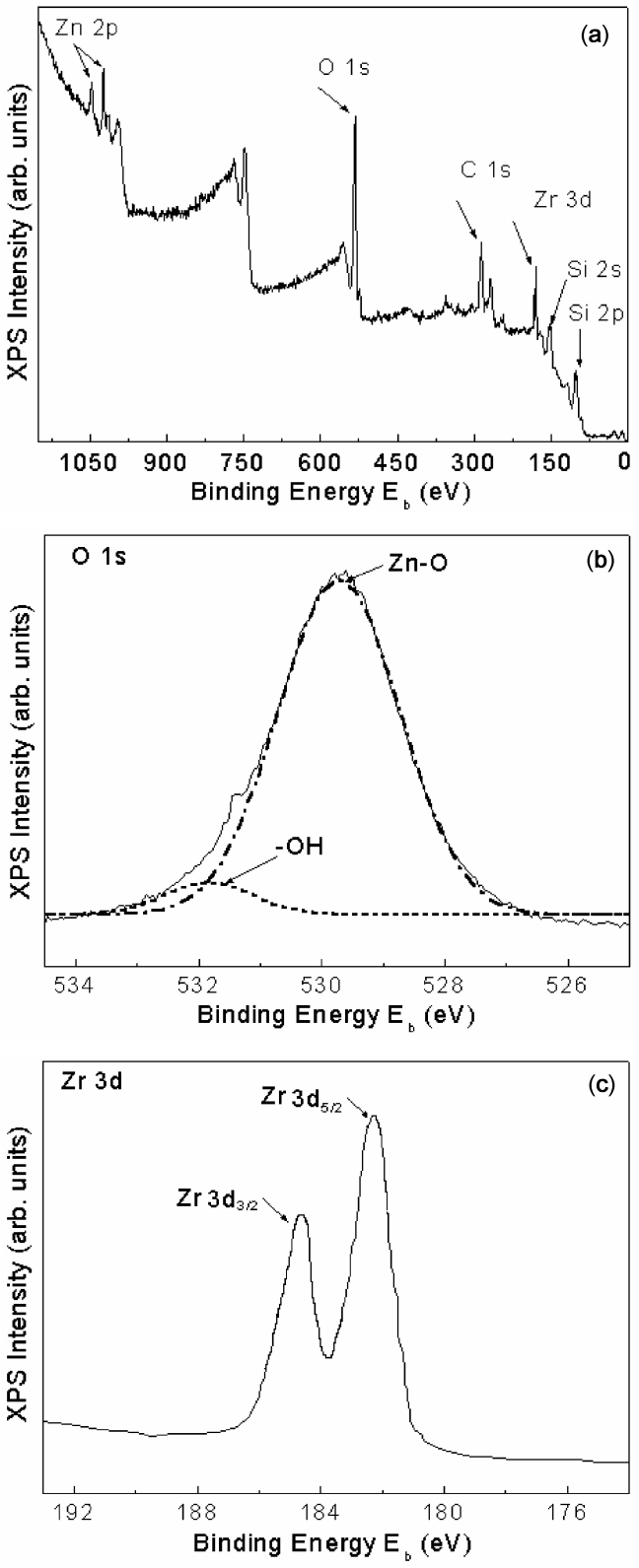

Figure 6. (**a**) Broad scan XPS spectrum of ZrO_2/ZnO/Si film showing characteristic peaks of Zn, O, C, Zr and Si, (**b**) deconvoluted O1 *s* and (**c**) typical Zr 3*d* spectra of ZrO_2/ZnO/Si film.

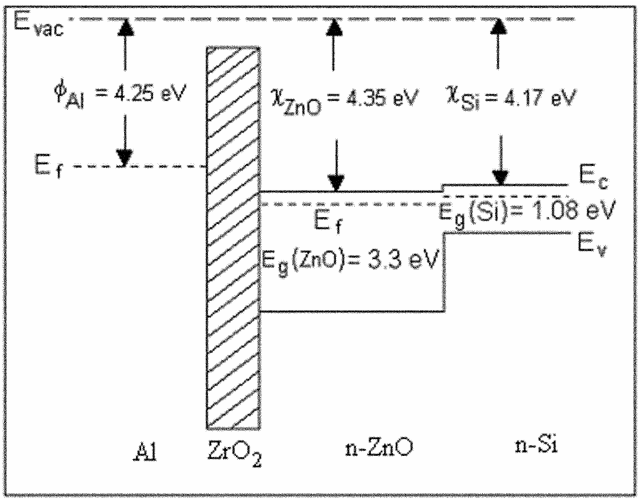

Figure 7. Energy band alignment in Al/ZrO_2/ZnO/*n*-Si MIS capacitor.

182·3 eV is a typical characteristic of the Zr^{4+} in ZrO_2 (Sun *et al* 2000).

The high frequency C–V characteristics of Al/ZrO_2/ZnO/*n*-Si in figure 8 (in inset) can be explained from the band diagram as shown in figure 7. From the band diagram it can be shown that the MIS capacitor will be in the inversion region at zero gate bias due to the favourable work function difference between the Al gate and ZnO. Interface trap density distribution throughout the band gap is evaluated by a high frequency method developed by Terman (1962). This method relies on capacitance–voltage measurement at a high frequency where interface traps are assumed not to respond to the a.c. signal but do respond to the varying d.c. voltages, and cause the C–V curve to stretch out along the voltage axis. This stretch-out effect produces a non-parallel shift of the C–V curve.

The interface trap density (D_{it}) is determined from the difference between the ideal and experimental ψ_s vs V_g curves by

$$D_{it} = \frac{C_{ox}}{q}\frac{d(\Delta V_g)}{d\psi_s}, \tag{1}$$

where ΔV_g is the voltage shift of the experimental curve with respect to ideal behaviour at each value of C, C_{ox} the oxide areal capacitance, ψ_s the surface potential, and q the electronic charge. An interface trap density of $2{\cdot}4 \times 10^{11}$ cm^{-2} eV^{-1} was calculated for the sample at midgap as shown in figure 8.

From the high frequency (1 MHz) capacitance–voltage characteristics presented in figure 8 (in inset), the depletion depth (X_{dHF}) and apparent doping (N_{appHF}) as a function of applied gate potential (V_G) are obtained as (Voinigescu *et al* 1994)

$$X_{dHF}(V_G) = \varepsilon_{ZnO} \cdot \left(\frac{1}{C_{HF}(V_G)} - \frac{1}{C_{ox}}\right), \tag{2}$$

$$\frac{1}{N_{appHF}(V_G)} = \frac{q\varepsilon_{ZnO}}{2} \cdot \frac{\delta\left(\frac{1}{C_{HF}^2(V_G)}\right)}{\delta V_G}, \tag{3}$$

where ε_{ZnO} is the ZnO permittivity, 9 (Sze 1979). C_{ox} is the gate oxide capacitance per unit area, $C_{HF}(V_G)$ the voltage dependent capacitance per unit area of the heterostructure, and q the electronic charge. The approximate substrate doping concentration (N_B) of $\approx 2{\cdot}5 \times 10^{15}$ cm^{-3} is obtained from a plot of N_{appHF} vs X_{dHF} as shown in figure 9(a). The threshold voltage of the ZnO/Si interface (V_{TH}) has been extracted from the C–V characteristics (figure 9(a)) and from the plot of N_{appHF} vs V (figure 9 (b)). The measured value of V_{th} is found to be –0·8 V.

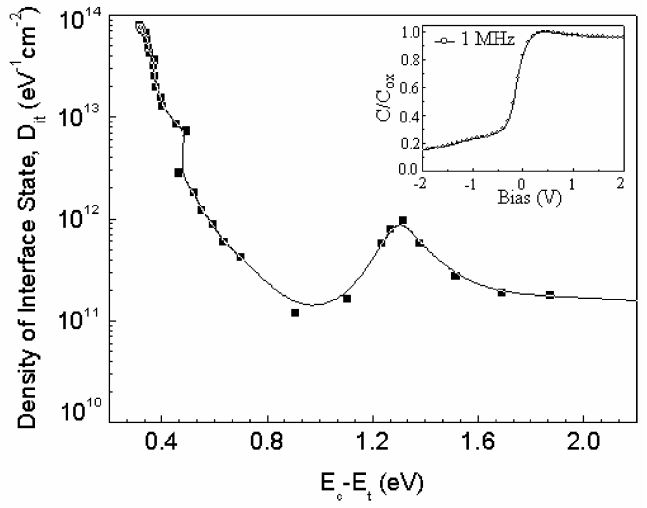

Figure 8. Energy distribution of density of interface states of Al/ZrO_2/ZnO/*n*-Si MIS capacitor (inset: high frequency C–V characteristics).

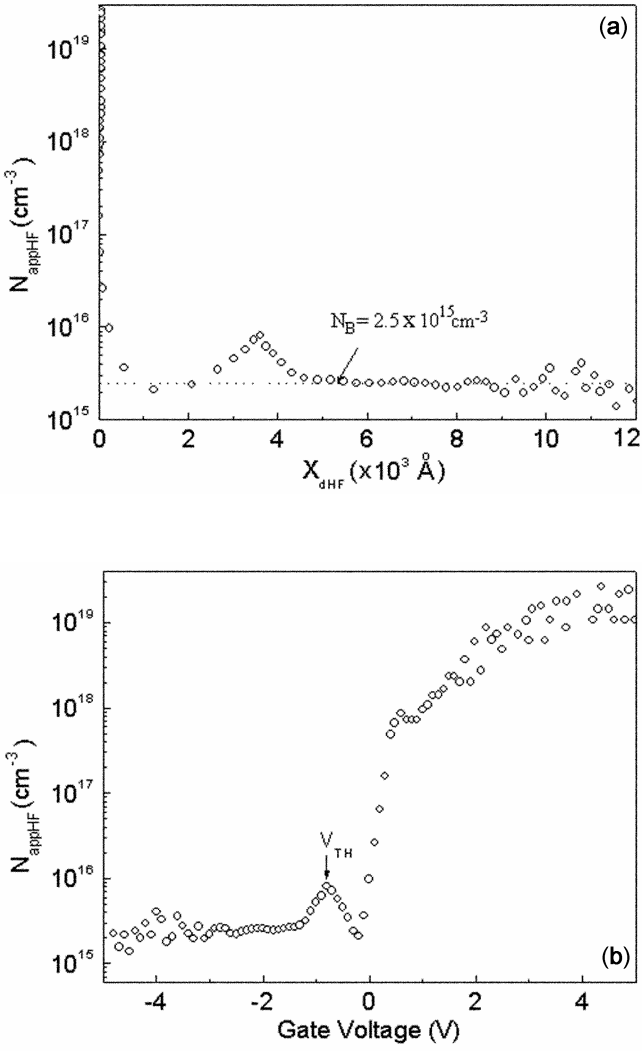

Figure 9. (**a**) Experimental apparent doping concentration vs distance from the ZnO/Si interface and (**b**) apparent doping vs gate voltage characteristics from the ZnO/Si interface.

To study the thermal stability of the dielectrics, high frequency (1 MHz) C–V and G–V were performed in the temperature range 27–200°C and the results are shown in figure 10. It is observed that the C–V and G–V curves shift towards the left as the device temperature is increased from 27–200°C. The flat band voltage (V_{fb}) is found to increase (more negative) with increasing device temperature as shown in figure 11, which indicates the generation of positive charges in the oxide. This may be due to the presence of hole trapping centres in the films.

The gate current density (J) as a function of voltage across the gate (V) for the ZrO_2/ZnO/n-Si layer is shown in figure 12(a), from room temperature up to 200°C. It is observed that the current density of the films is strongly temperature dependent at low field, i.e. for $E < 1$ MV/cm, while its temperature dependence is much weaker at higher voltage. In figure 12(b), we show the temperature dependence of the conductance current at two electric fields, 0·4 MV/cm and 2·7 MV/cm (Yassine *et al* 1999), respectively. This is also known as Arrhenius plot. The Schottky

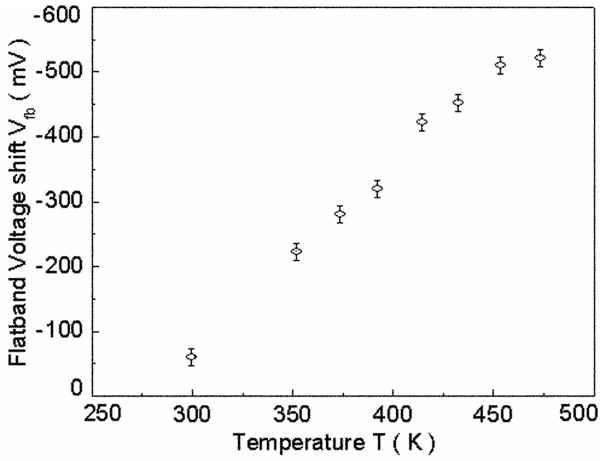

Figure 11. Flat band voltage shift vs temperature characteristics.

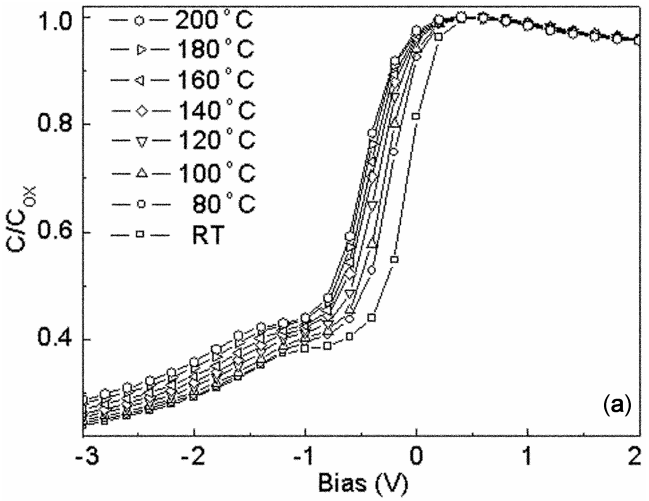

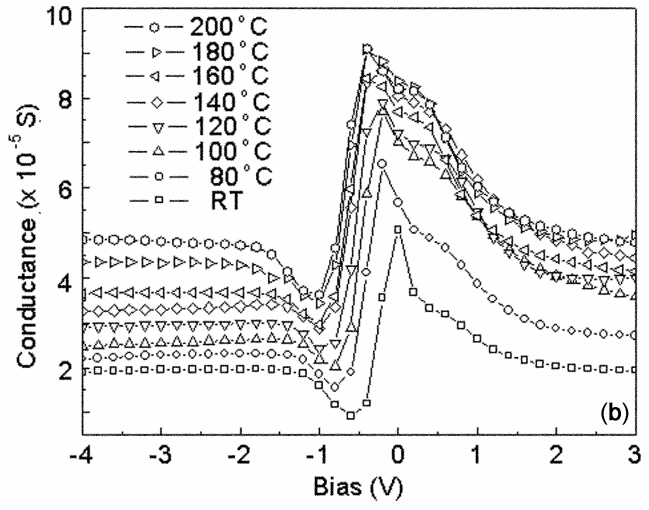

Figure 10. High temperature measurement of (**a**) normalized capacitance and (**b**) conductance for MOS capacitors on ZnO films.

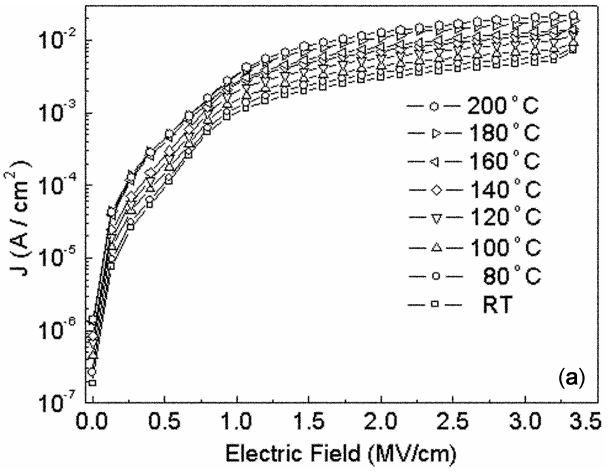

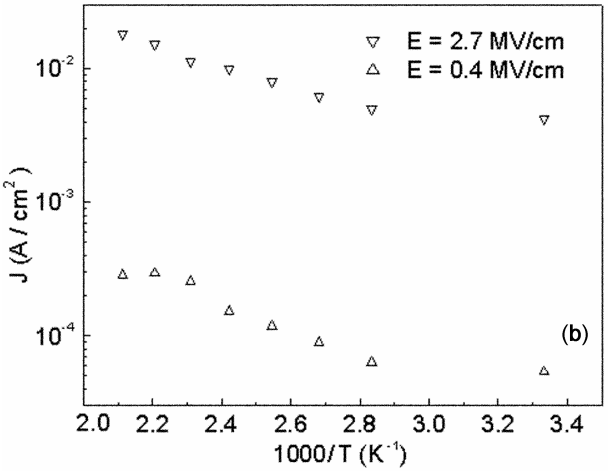

Figure 12. Current density, J, as a function of electric field across the gate dielectric of Al–ZrO_2–ZnO/n-Si MOS capacitors: (**a**) recorded at room temperature to 200°C and (**b**) current density, J vs inverse of temperature for fixed applied electric fields, E, of 0·4 MV/cm and 2·7 MV/cm, respectively.

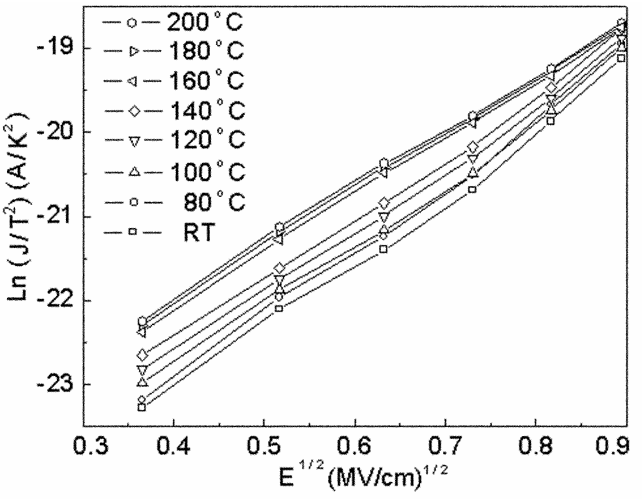

Figure 13. The $\ln J/T^2$ vs $E^{1/2}$ plot for a MIS capacitor at different temperatures showing Schottky conduction.

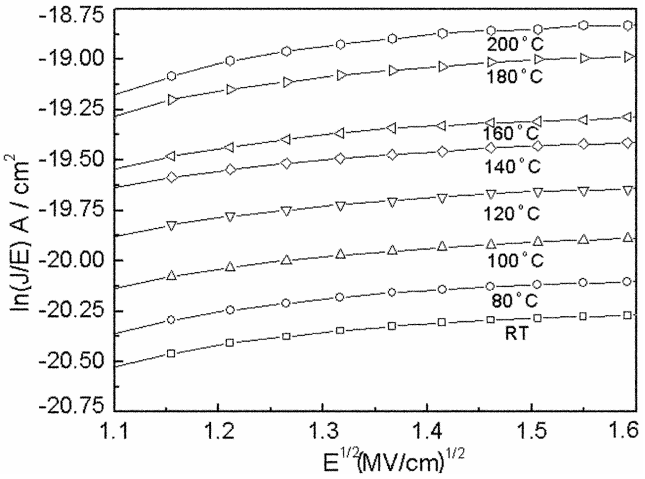

Figure 14. The $\ln(J/E)$ vs $E^{1/2}$ is plotted for the MIS capacitor. The straight line characteristic at relatively high electric field (≤ 1·1 MV/cm) indicates Poole–Frenkel conduction.

emission (SE), Poole–Frenkel (PF) emission, FN tunneling, direct tunneling and space-charged limited mechanism are used to explain the basic conduction process in insulators. The SE process is due to the thermionic emissions across the metal–insulator-interface, which is responsible for carrier transport.

The thermionic emission models range in various levels of physical complexity. The Schottky–Richardson relation is given for the *J–E* relation for Schottky emission,

$$J = C_{\mathrm{RD}} \cdot T^2 \cdot \exp\left[\frac{-q\Phi_{\mathrm{b}}}{kT}\right] \cdot \exp\left[\frac{\beta \cdot \sqrt{E}}{kT}\right], \tag{4}$$

where $\beta = \sqrt{q^3 / 4\pi\varepsilon_0\varepsilon_{\mathrm{i}}}$ and C_{RD} the Richardson constant. Equation (4) can be written as

$$\ln(J/T^2) = \ln(C_{\mathrm{RD}}) - \frac{q\Phi_{\mathrm{b}}}{kT} + \frac{\beta \cdot \sqrt{E}}{kT}. \tag{5}$$

The plot of $\ln(J/T^2)$ vs $\sqrt{E}$ is a straight line with a slope, β/kT. From figure 13, one can observe that the experimental plot of $\ln(J/T^2)$ vs $\sqrt{E}$ with temperature as a parameter is a straight line, which follows the SE mechanism at low electric field (≤0·65 MV/cm). The conduction properties of these films were further studied by plotting the data in terms of PF mechanism (Sze 1979) at higher electric fields. When the top electrode (gate) is positively biased, i.e. the holes are injected from the gate, the leakage current in the films can be well fitted by $\ln(J/E)$ vs $E^{1/2}$ plot, indicating that the conduction is PF mechanism in the high field range (1·10–1·60 MV/cm) as shown in figure 14.

4. Conclusions

In summary, undoped polycrystalline ZnO (100 nm) thin films were deposited on *n*-Si (100) at 450°C by rf magnetron sputtering. It is shown that the low temperature microwave PECVD techniques are useful for the deposition of good quality high-*k* ZrO_2 gate dielectric directly on ZnO/*n*-Si for future MIS applications. High temperature conduction mechanism is found to be dominated by Schottky emission at low electric field while the Poole–Frenkel emission takes over at high electric field.

Acknowledgement

The ZnO/Si samples were prepared by Dr S Maikap.

References

Ayouchi R, Leinen D, Martin F, Gabas M, Dalchiele E and Barrado J R R 2003 *Thin Solid Films* **426** 68

Bachari E M, Amor S B, Baud G and Jacquet M 2001 *Mater. Sci. Eng.* **B79** 165

Bagnall D M, Chen Y F, Zhu Z, Yao T, Koyama S, Shen M Y and Goto T 1997 *Appl. Phys. Lett.* **70** 2230

Balog M, Schieber M, Michman M and Patai S 1977 *Thin Solid Films* **47** 109

Cameron M A and George S M 1999 *Thin Solid Films* **348** 90

French R H, Glass S J, Ohuchi F S, Xu Y N and Ching W Y 1994 *Phys. Rev.* **B49** 5133

Gorla C R, Emanetoglu N W, Liang S, Mayo W E, Lu Y, Wraback M and Shen H 1999 *J. Appl. Phys.* **85** 2595

Jeong W J, Kim S K and Park G C 2006 *Thin Solid Films* **506–507** 180

Khawaja E E, Bouamrane F, Hallak A B, Daous M A and Salim M A 1993 *J. Vac. Sci. & Technol.* **A11** 580

Kralik B, Chang E K and Louie S G 1998 *Phys. Rev.* **B57** 7027

Kubo M, Oumi Y, Takaba H, Chatterjee A, Miyamoto A, Kawasaki M, Yoshimoto M and Koinuma H 2000 *Phys. Rev.* **B61** 16187

Liu Y, Gorla C R, Liang S, Emanetoglu N, Lu Y, Shen H and Wraback M 2000 *J. Electron. Mater.* **29** 60

Marotti R E, Guerra D N, Bello C, Machado G and Dalchiele E A 2004 *Sol. Energy Mater. & Sol. Cell* **82** 85

Nandi S K *et al* 2002 *Electron. Lett.* **38** 1390

Raoux S, Cheung D, Fodor M, Taylor W N and Fairbairn K 1997 *Plasma Sources Sci. Technol.* **6** 405

Ray S K, Maiti C K, Lahiri S K and Chakrabarti N B 1996 *Adv. Mater. Opt. Electron.* **6** 73

Russak M A, Jahnes C V and Katz E P 1989 *J. Vac. Sci. & Technol.* **A7** 1248

Shi C, Fu Z, Guo C, Ye X, Wei Y, Deng J, Shi J and Zhang G 1999 *J. Electron. Spectrosc. & Rel. Phenom.* **101–103** 629

Sun Y M, Lozano J, Ho H, Park H J, Veldman S and White J M 2000 *Appl. Surf. Sci.* **61** 115

Sze S M 1979 *Physics of semiconductor devices* (Wiley Eastern Limited)

Tanaka S, Takahashi K, Sekiguchi T, Sumino K and Tanaka J 1995 *J. Appl. Phys.* **77** 4021

Tang Z K, Kawasaki M, Ohtomo A, Koinuma H and Segawa Y 2006 *J. Cryst. Growth* **287** 169

Terman L M 1962 *Solid State Electron.* **5** 285

Vanheusden K, Warren W L, Seager C H, Tallant D R, Voigt J A and Gnade B E 1996 *J. Appl. Phys.* **79** 7983

Voinigescu S P, Iniewski K, Lisak R, Salama C A T, Noel J P and Houghton D C 1994 *Solid State Electron.* **37** 1491

Xu W, Ye Z, Zhu L, Zeng Y, Jiang L and Zhao B 2005 *J. Cryst. Growth* **277** 490

Yassine A, Nariman H E and Olasupo K 1999 *IEEE Electron. Dev. Lett.* **20** 390